Supplementary Information

Understanding Photocatalytic Hydrogen Peroxide Production in Pure Water for Benzothiadiazole-based Covalent Organic Frameworks

Linyang Wang[a], Jiamin Sun[a], Maojun Deng[a], Chunhui Liu[a], Servet Ataberk Cayan[b,c], Korneel Molkens[b,c], Pieter Geiregat[b,c], Rino Morent[d], Nathalie De Geyter[d], Jeet Chakraborty[a]*, Pascal Van Der Voort[a]*

[a] COMOC − Center for Ordered Materials, Organometallics and Catalysis, Department of Chemistry, Ghent University, Krijgslaan 281-S3, 9000 Ghent, Belgium.
[b] Physics and Chemistry of Nanostructures, Department of Chemistry, Ghent University, Krijgslaan 281-S3, 9000 Ghent, Belgium.
[c] NOLIMITS, Center for Non-Linear Microscopy and Spectroscopy, Ghent University, Krijgslaan 281-S3, 9000 Ghent, Belgium.
[d] RUPT − Research Unit Plasma Technology, Department of Applied Physics, Ghent University, Sint-Pietersnieuwstraat 41 B4, 9000 Gent, Belgium.

Email: pascal.vandervoort@ugent.be; jeet.chakraborty@ugent.be

The apparent quantum yield (AQY) measurement

The apparent quantum yield of TAPT-BT-COF was measured under 300 W Xe lamp irradiation (with a bandpass glass filter of 420 nm). The light intensity at 420 nm is measured by an optical power meter. The AQY was calculated as follows:

$$AQY(\%) = \frac{(Number\ of\ produced\ H_2O_2\ molecules) \times 2}{number\ of\ incident\ photons} \times 100$$
$$= \frac{(Number\ of\ produced\ H_2O_2\ molecules) \times 2}{ISt\lambda/hc} \#(1)$$

Where I = light power intensity (W cm^{-2}); S = the irradiation area (cm^2); t = reaction time (s); λ = wavelength (m); h = 6.63×10^{-34} m^2 kg s^{-1}(Planck's constant); c = 3×10^8 m s^{-1} (speed of light).

Electrode preparation

To prepare the working electrodes, 5 mg ground sample was dispersed in 1 mL as-prepared solution (ethanol: Nafion =100:1). After sonication for 10 min, the solution was dropped on the surface of FTO glass with an exposed area of 1× 1 cm^2, and then dried in air at 40˚C. This step was repeated three times to achieve a uniform coverage.

Transmission electron microscopy (TEM) and scanning transmission electron microscopy energy-dispersive X-ray spectroscopy (STEM-EDS) mapping

The samples were dispersed in ethanol at room temperature and drop cast on an amorphous carbon coated Cu TEM grid. TEM images were collected on a JEOL JEM-2200FS transmission electron microscope with a HAADF detector, and operated at 200 kV and equipped with a C_s corrector. The composition of the materials was studied using EDS in the HAADF-STEM mode.

Electrochemical impedance spectroscopy (EIS) and Mott-Schottky measurement

All electrochemical measurements were performed in a standard three-electrode system. Pt foil served as the counter electrode and Ag/AgCl was used as reference electrode. The working electrodes were immersed in the electrolyte for 60 s before any measurement was conducted. Impedance measurements were collected in a 0.1 mol/L Na_2SO_4 solution at a bias potential of -0.5 V over a frequency range from 10^6 to 10^{-1} Hz. The photocurrents were tested under 300 W Xe lamp irradiation with light on-off cycles at a time interval of 30 s and the scan rate was 150 mV/s, while the working electrodes were irradiated from the back side to minimize the influence of the thickness of the semiconductor layer. The Mott–Schottky plotswith frequency of 1 kHz, 2 kHz, 3 kHz in dark condition to determine the flat-band potential. The applied potentials vs.

Ag/AgCl were converted to NHE (Normal Hydrogen Electrode) or RHE (Reversible Hydrogen Electrode) potentials using the following equations:

$$E_{NHE} = E_{Ag/AgCl} + E^{\theta}_{Ag/AgCl} \left(E^{\theta}_{Ag/AgCl} = 0.199\,V\right) \#(2)$$

$$E_{RHE} = E_{Ag/AgCl} + 0.0591pH + E^{\theta}_{Ag/AgCl} \left(E^{\theta}_{Ag/AgCl} = 0.199\,V\right) \#(3)$$

Quantification of H_2O_2

The concentration of H_2O_2 was quantified using the Ti reagent solution by UV-visible spectroscopy. An aqueous Ti reagent solution was prepared by diluting 640 mg of Titanium (IV) oxysulfate-sulfuric acid hydrate in sulfuric acid (40 mL, 16 M) with milli-Q water to give 750 mL of solution ($TiOSO_4.xH_2O+H_2SO_4$). This acidic aqueous solution of titanium oxysulfate reacts in the presence of H_2O_2, resulting in the formation of a yellow peroxotitanium complex $[Ti(O_2)OH(H_2O)_3]^+_{aq}$(Eq. S4-5), the absorbance of which can be measured at 409 nm.

$$TiOSO_{4(s)} + 5H_2O \leftrightarrow [Ti(OH)3(H2O)3] + (aq) + HSO_4^-(aq) \quad (\text{Eq. S4})$$

$$[Ti(OH)3(H2O)3] + (aq) + H2O2\,(aq) \leftrightarrow [Ti(O2)OH(H2O)3] + (aq) + 2H_2O \quad (\text{Eq. S5})$$

After the photocatalytic reaction, we transferred 1 mL of sample solution (after syringe filtration to remove photocatalysts) into a quartz tube and then add 1 mL of Ti reagent solution. Then measure the absorbance of this solution by using Shimadzu UV-1800 UV-visible scanning spectrophotometer (see Fig. S19).

Zeta potential measurement

The isoelectric point was determined using a Malvern Panalytical Zetasizer Ultra equipped by zeta potential measurements. To this end, 2 mg of COFs was dispersed in 2 ml Milli-Q water and sonicated for 1 h to give a mixed solution. Then 1 ml of mixed solution was used for a zetapotential titration measurement. The pH was adjusted to either acidic or basic values using aqueous HCl (0.01 M) or aqueous NaOH (0.01 M) respectively, starting each time from the natural pH to minimise salt loading.

Femtosecond transient absorption (TA) spectroscopy

TA experiments are carried out using a 5 kHz Yb:KGW laser source (1030 nm, Carbide, Light Conversion) where pump light is generated through third harmonic generation in a sequence of BBO crystals and probe light is generated by focusing the fundamental into a sapphire crystal of 5 mm thickness. In short, a 220 fs pump pulse at 343 nm excites a thin film of the COF system under ambient conditions. At a time delay *t* (0-1000 ps) generated through a mechanical delay line, a broadband probe pulse measures the change in absorption ΔA over the wavelength range from 525 to 850 nm. Due to the

high optical density (OD) of the film above the band gap, no direct bleach of the band gap transitions can be observed in transmission.

Theoretical studies

The theoretical HOMO-LUMO of the materials and free-energy calculations for the catalysis were conducted on BIOVIA Materials Studio. The molecular orbitals of TAPT-BT and TAPB-BT were obtained by the VAMP module using AM1 Hamiltonian and Restricted Hartee-Fock methods. The geometry and energy optimized structures were used to calculate their electron density and potential energy surface. The same module was used to further optimize the geometry and energy of the reaction intermediates, followed by their thermodynamic properties' computation at 298 K. The free-energy change (ΔG) was calculated at this temperature (T) from the computed change in enthalpy (ΔH) and entropy (ΔS) using the equation $\Delta G = \Delta H + T\Delta S$

Synthesis of 4,4'-(benzothiadiazole-4,7-diyl)dibenzaldehyde (BT)

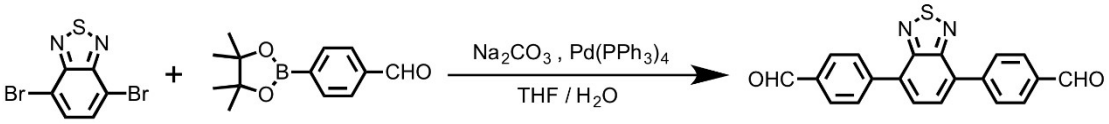

4,4'-(benzothiadiazole-4,7-diyl)dibenzaldehyde was synthesized according to a previously reported procedure[1]. Generally, 4,7-dibromo-2,1,3-benzothiadiazole (4 mmol, 1.18 g), 4-formylphenylboronic acid (12 mmol, 1.8 g) sodium carbonate (24 mmol, 2.55 g), and tetrakis(triphenylphosphine)palladium(0) were introduced into a 100 mL three-neck flask and degassed for three times. Then, dioxane/water (50 mL, v/v = 4/1) was slowly added into the flask under a N_2 atmosphere. After reflux for 48h under N_2, the mixture was poured into distilled water. The yellow solid was filtered and washed with water giving the crude compound which was further purified by flash chromatography with dichloromethane as eluent to afford the title product as a yellowish green powder (1.03 g, 73%). ^{1}H NMR (400 MHz, $CDCl_3$): δ 10.07 (s, 2H, CHO), 8.12 (d, 4H, Ph-H), 8.02 (d, 4H, Ph-H), 7.85 (s, 2H, Ph-H) ppm.

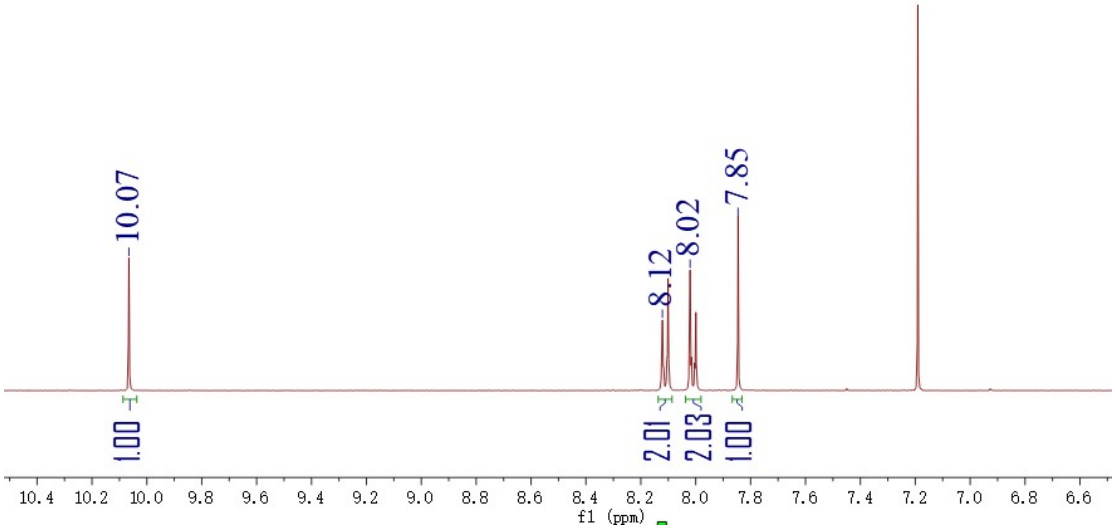

Fig. S1 ^{1}H NMR spectrum of 4,4'-(Benzothiadiazole-4,7-diyl)dibenzaldehyde (BT) in $CDCl_3$ (The peak at 7.2 ppm originates from $CDCl_3$).

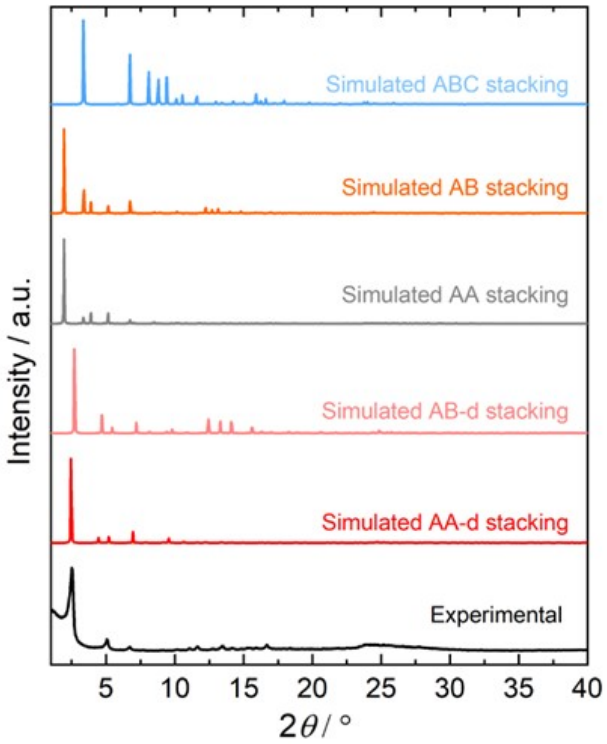

Fig. S2 Comparison of the experimental PXRD pattern of TAPT-BT-COF with the simulated possible stacking models, where the AA-d, AB-d, AA, AB, and ABC stackings are related to the formation of regular hexagonal pores. The AA-d stacking model represents the distortions of TAPT-BT-COF.

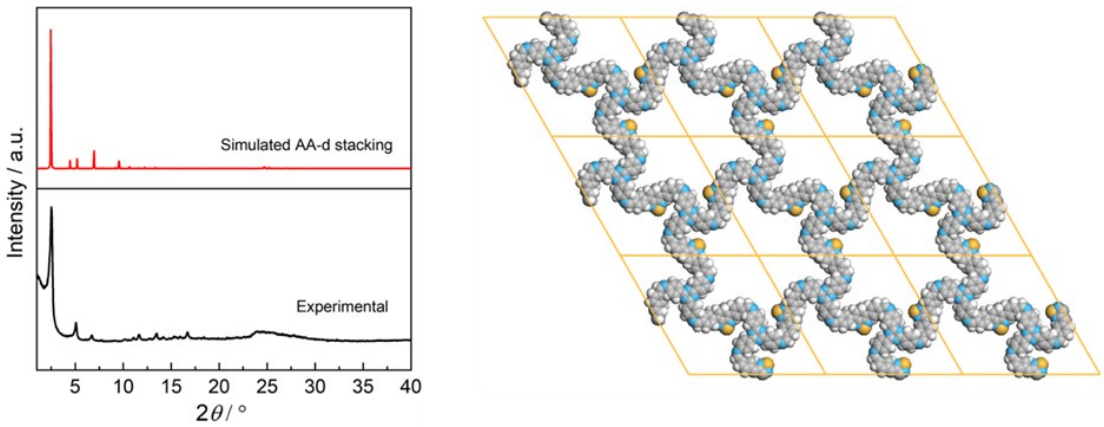

Fig. S3 Comparison of the experimental (black) and simulated AA-d stacking PXRD patterns of TAPT-BT-COF and the top view of the simulated structure of AA-d stacking.

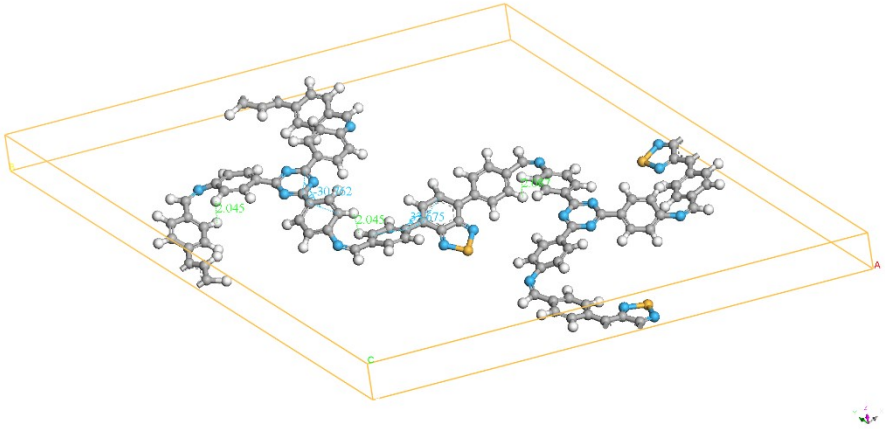

Fig. S4 Localized unit cell structure of TAPT-BT-COF in AA-d stacking to demonstrate the rotation (ca. 30°) of the benzene rings due to repulsion between hydrogen atoms.

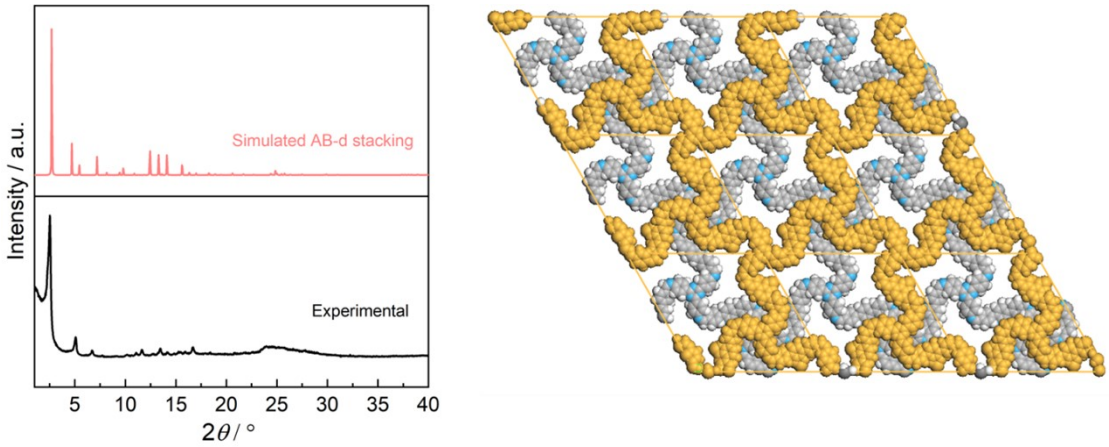

Fig. S5 Comparison of the experimental (black) and simulated AB-d stacking PXRD patterns of TAPT-BT-COF and the top view of the simulated structure of AB-d

stacking.

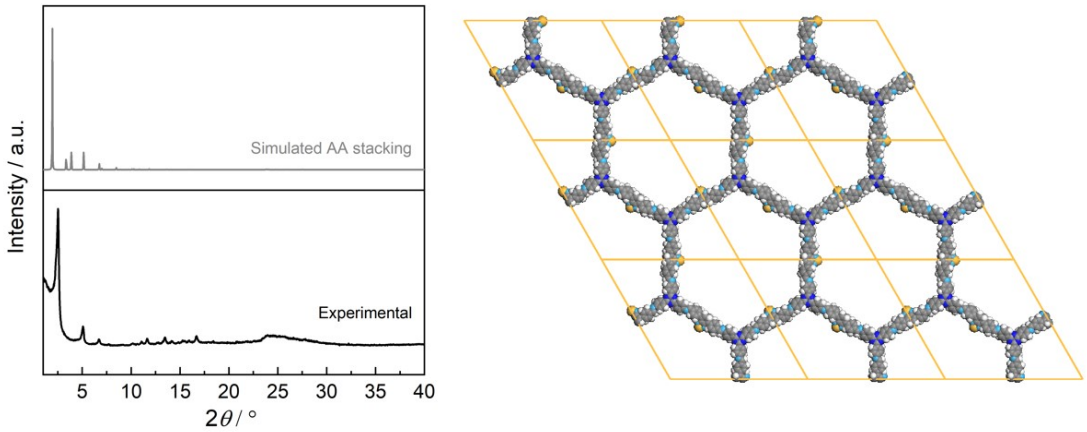

Fig. S6 Comparison of the experimental (black) and simulated AA stacking PXRD patterns of TAPT-BT-COF and the top view of the simulated structure of AA stacking.

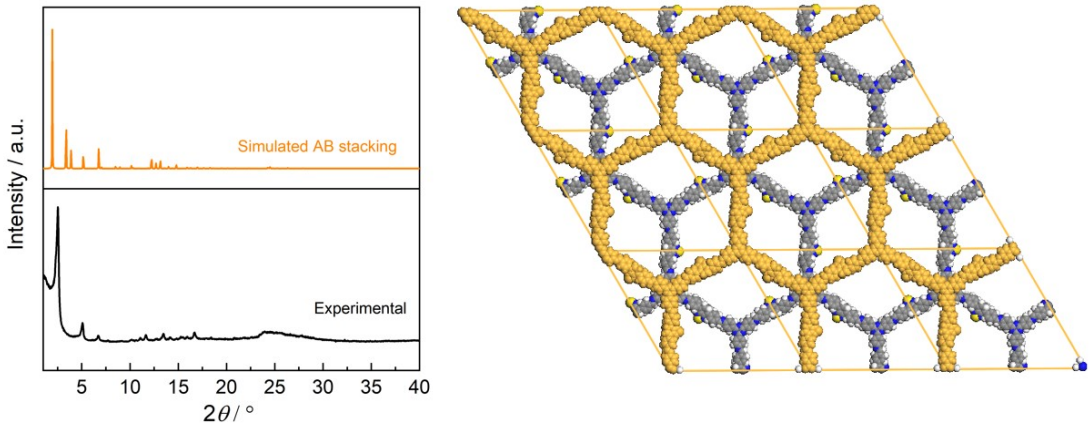

Fig. S7 Comparison of the experimental (black) and simulated ABC stacking PXRD patterns of TAPT-BT-COF and the top view of the simulated structure of ABC stacking.

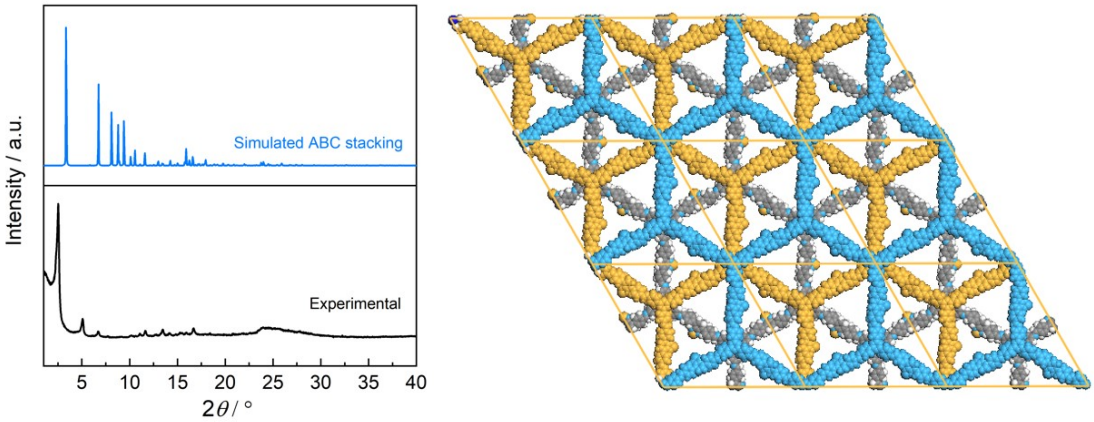

Fig. S8 Comparison of the experimental (black) and simulated ABC stacking PXRD patterns of TAPT-BT-COF and the top view of the simulated structure of ABC stacking.

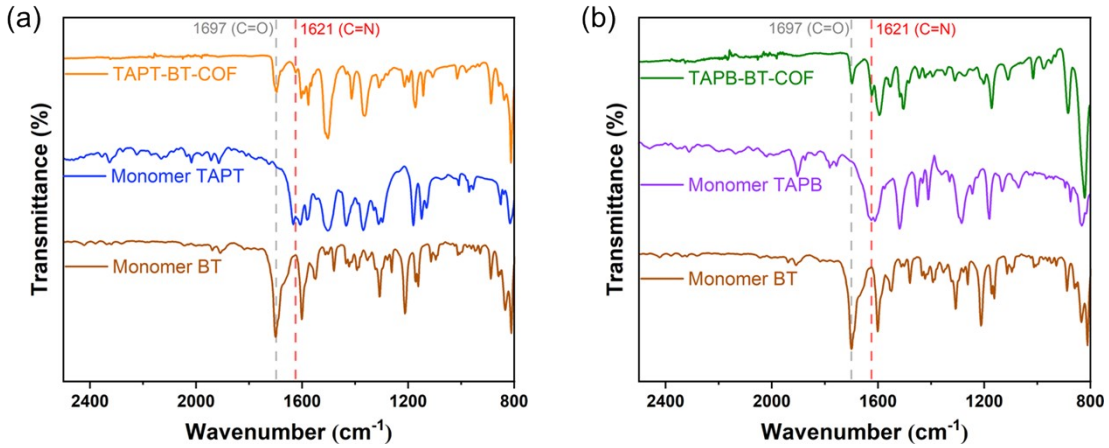

Fig. S9 FT-IR spectra of TAPT-BT-COF and TAPB-BT-COF and their monomers.

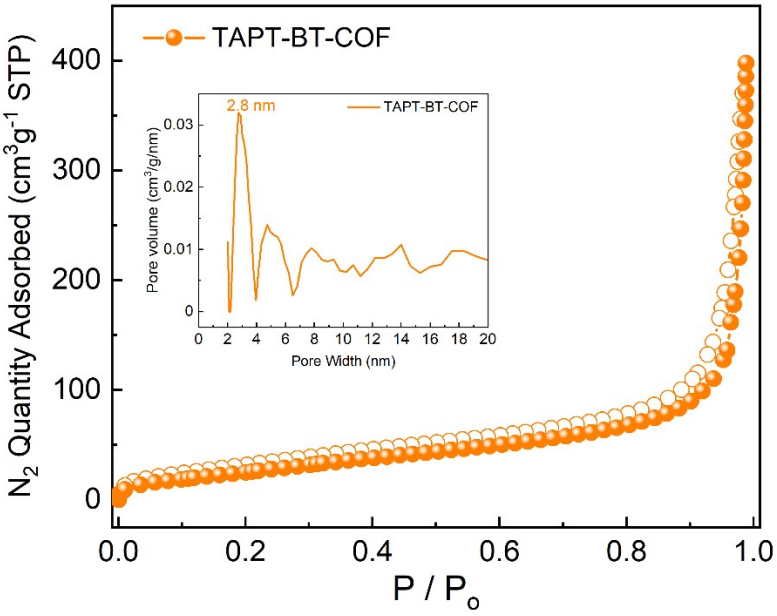

Fig. S10 N_2 adsorption-desorption analyses and pore size distribution of TAPT-BT-COF

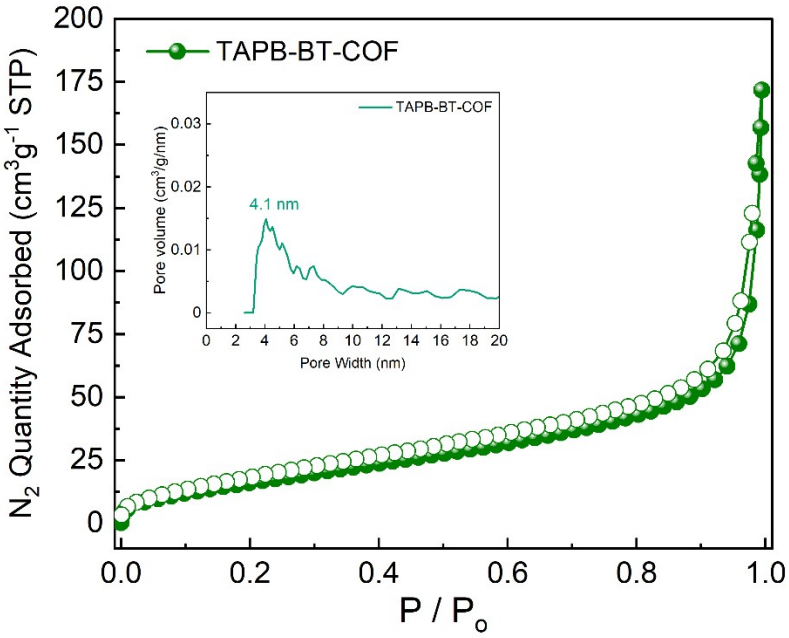

Fig. S11 N_2 adsorption-desorption analyses and pore size distribution of TAPB-BT-COF

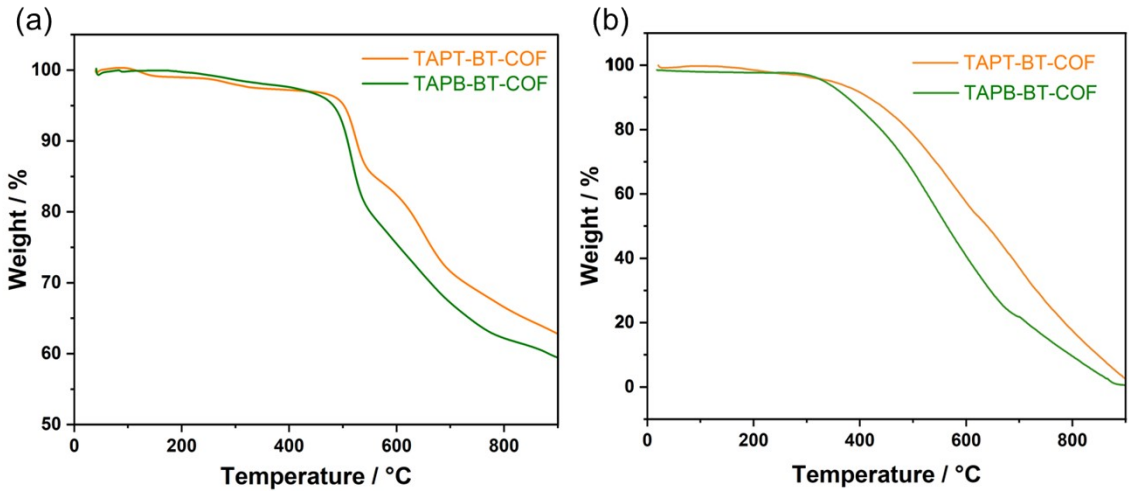

Fig. S12 TGA curves of TAPT-BT-COF and TAPB-BT-COF under (a) N_2 and (b) air.

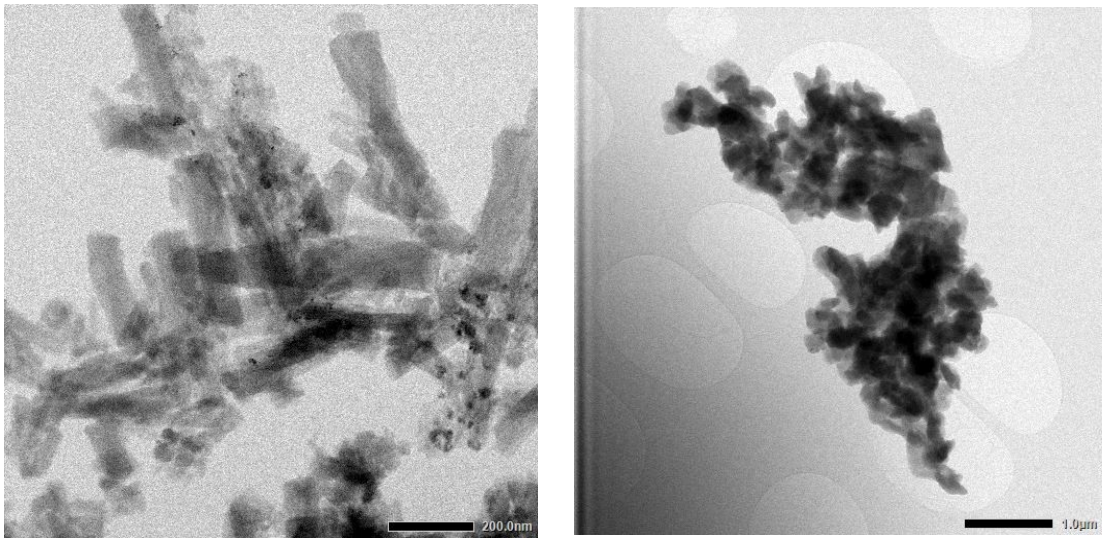

Fig. S13 TEM images of TAPT-BT-COF (left) and TAPB-BT-COF (right).

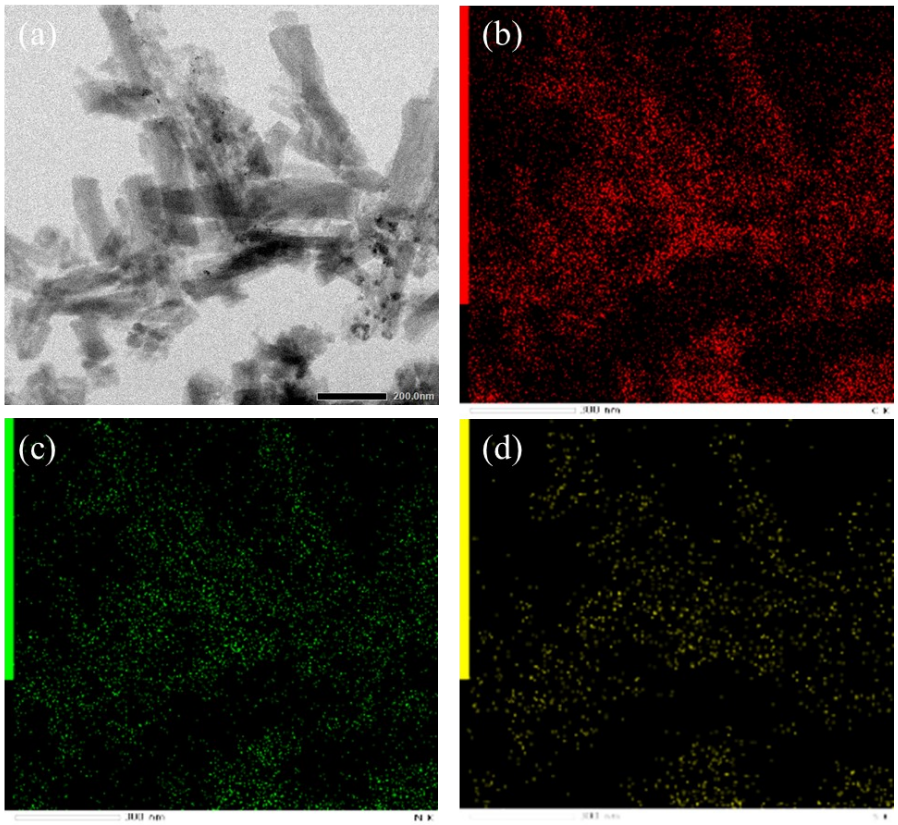

Fig. S14 STEM-EDS element mapping of TAPT-BT-COF. (a) TEM image, (b) Carbon element, (c) Nitrogen element and (d) Sulfur element.

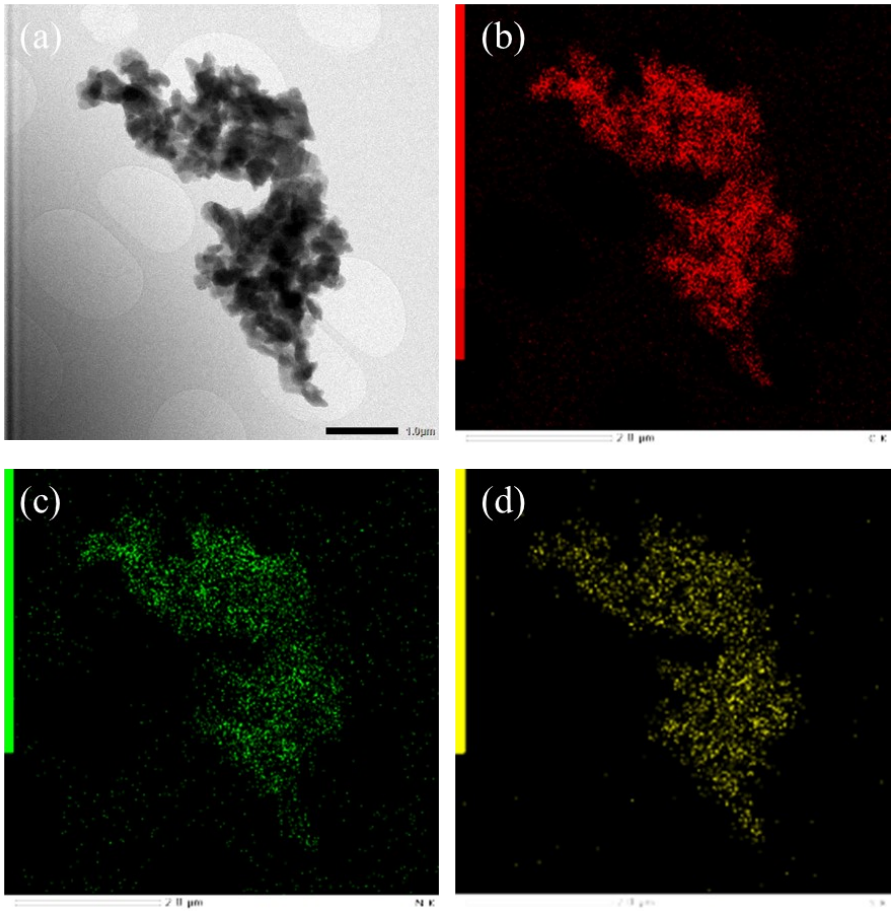

Fig. S15 STEM-EDS element mapping of TAPB-BT-COF. (a) TEM image, (b) Carbon element, (c) Nitrogen element and (d) Sulfur element.

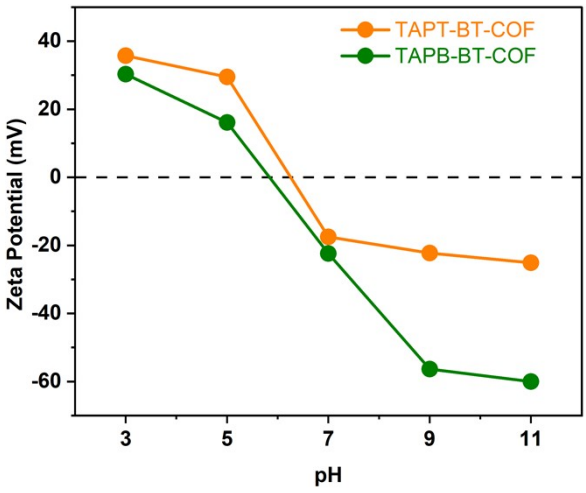

Fig. S16 Zeta potential of TAPT-BT-COF and TAPB-BT-COF as a function of pH showing the isoelectric point of the COFs around pH 6.

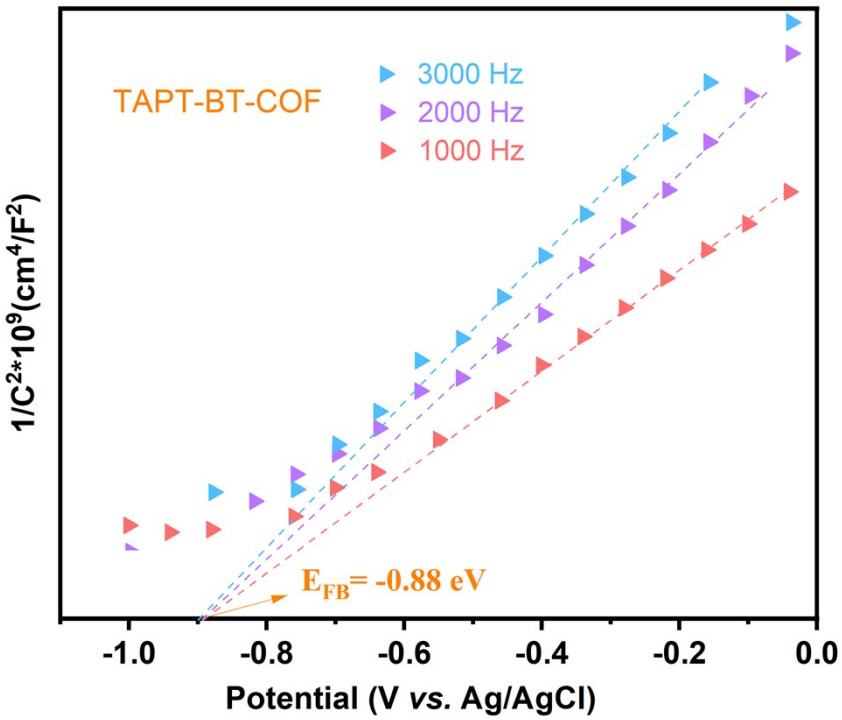

Fig. S17 Mott-Schottky plots of TAPT-BT-COF.

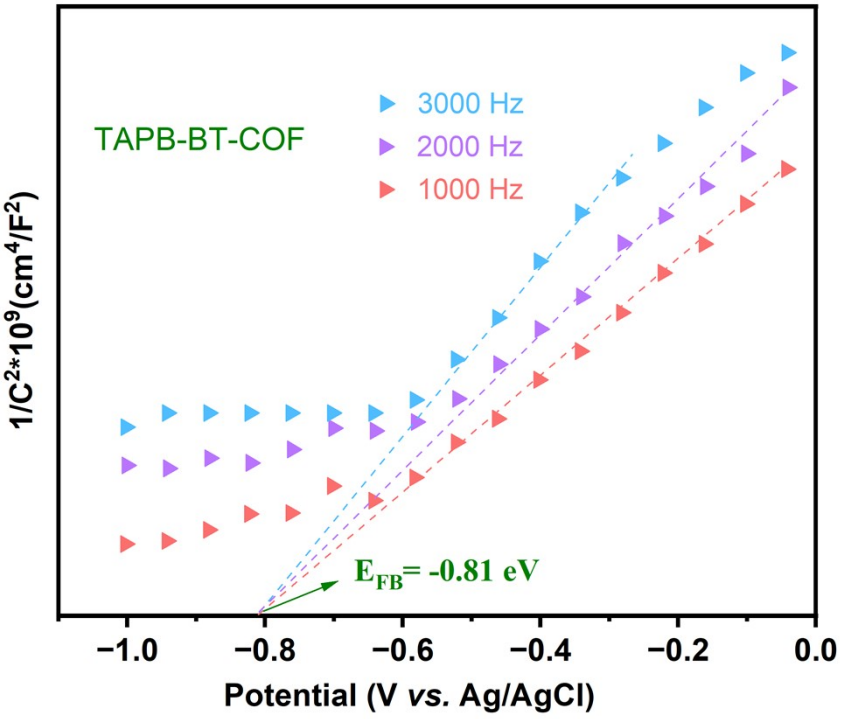

Fig. S18 Mott-Schottky plots of TAPB-BT-COF.

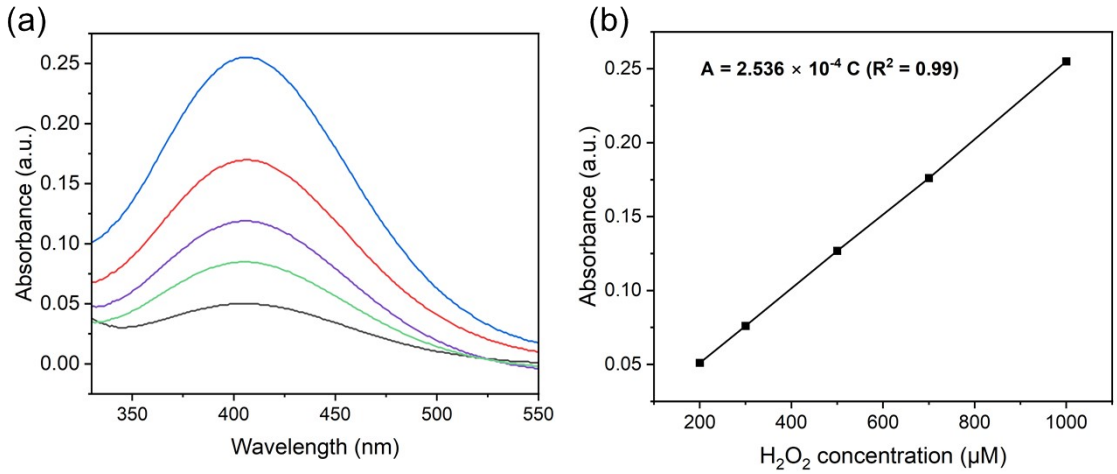

Fig. S19 (a) The adsorption spectra of different concentrations of H_2O_2 in the presence of Ti reagent solution at wavelengths of 325-550 nm. (b) The H_2O_2 concentration-absorbance calibration curve.

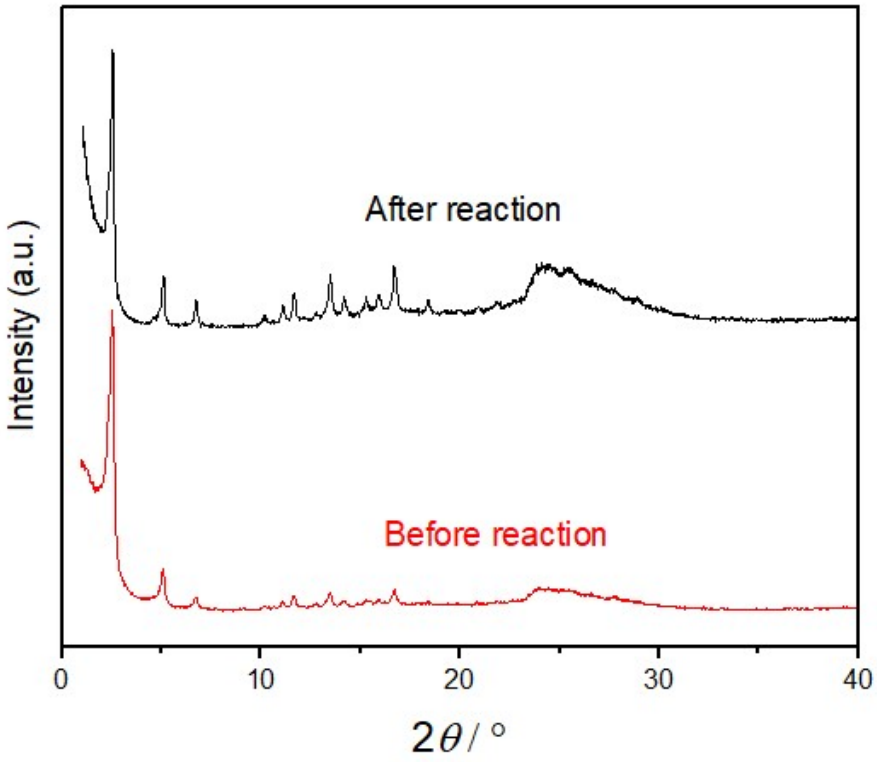

Fig. S20 PXRD patterns of TAPT-BT-COF before and after catalysis.

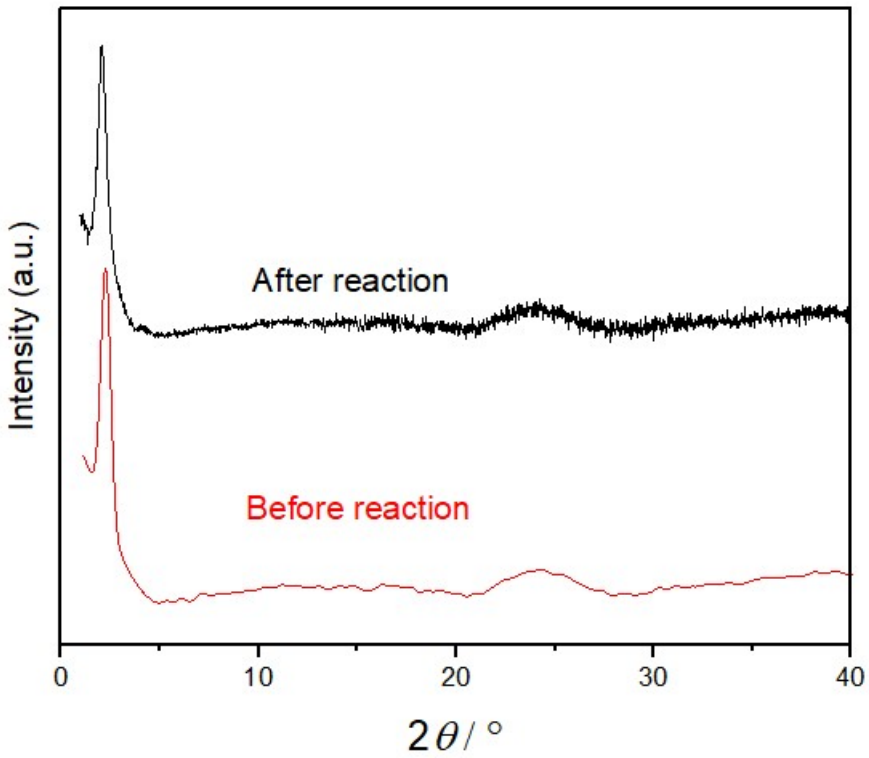

Fig. S21 PXRD patterns of TAPB-BT-COF before and after catalysis.

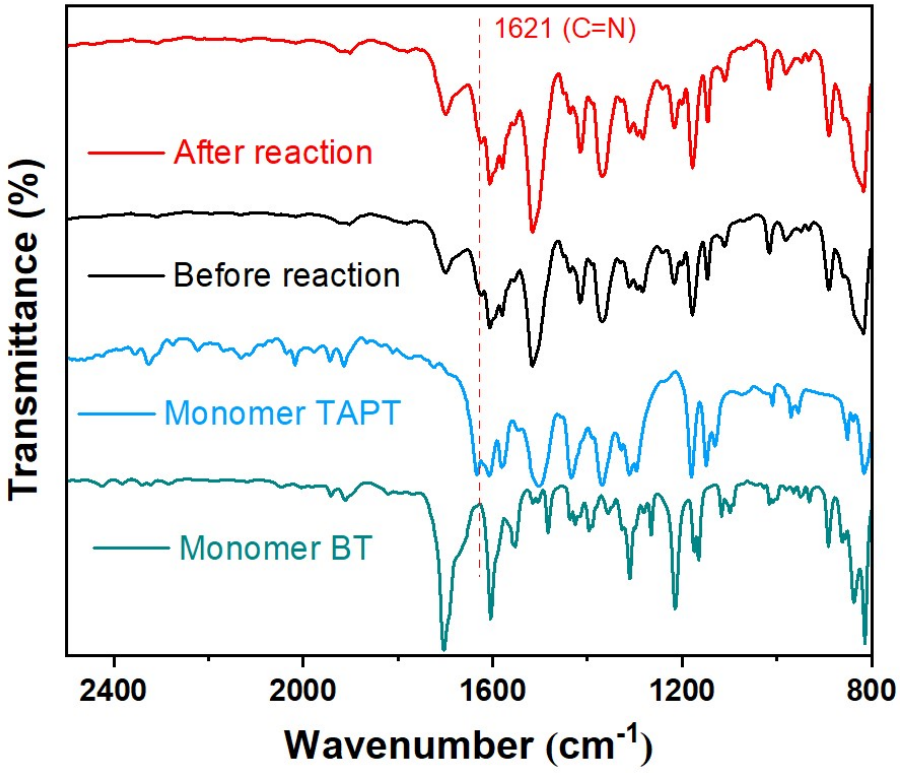

Fig. S22 FTIR of TAPT-BT-COF before and after catalysis.

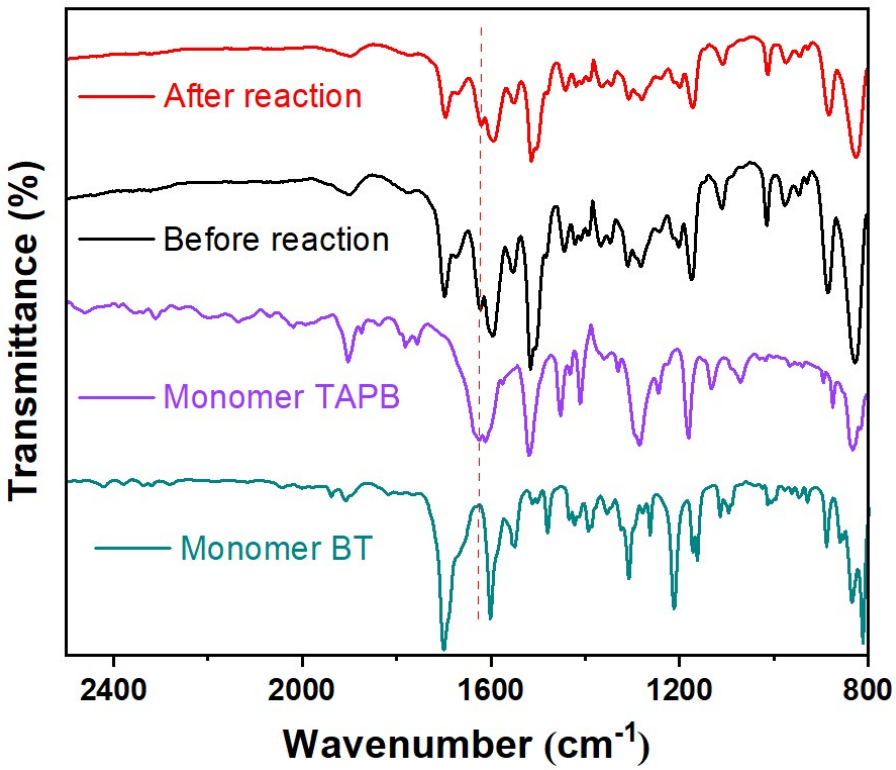

Fig. S23 FTIR of TAPB-BT-COF before and after catalysis.

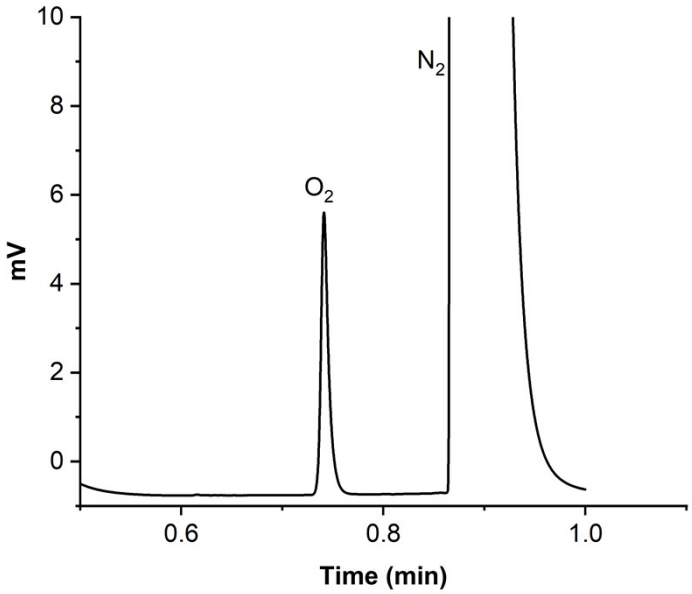

Fig. S24 GC chromatogram of TAPT-BT-COF. A vial was charged with 3 mM $AgNO_3$ aqueous solution (5 mL) and 10 mg COF. Oxygen is removed by bubbling N_2 in dark condition. Before starting the reaction, the gas headspace of the vial was measured by GC to ensure that no oxygen was present in the vial.

Tab. S1 The charge transfer resistance (R_{CT}) and the bulk resistance (R_{Bulk}) of the COFs.

Material	R_{bulk} (Ω)	R_{CT} (Ω)
TAPT	32	299
TAPB	43.3	1255

Tab. S2 Comparison with other representative materials in photocatalytic H_2O_2 production.

Material	H_2O_2 production rate	Irradiation conditions	Solvent	Reference
TAPD-$(Me)_2$-COF	97 μmol g^{-1} h^{-1}	λ > 420 nm	H_2O: EtOH = 9:1	1
TAPD-$(OMe)_2$-COF	91 μmol g^{-1} h^{-1}	λ > 420 nm	H_2O: EtOH = 9:1	1
H-COF	516 μmol g^{-1} h^{-1}	λ > 400 nm	H_2O: EtOH = 9:1	2
TF-COF	1239 μmol g^{-1} h^{-1}	λ > 400 nm	H_2O: EtOH = 9:1	2
TF_{50}-COF	1739 μmol g^{-1} h^{-1}	λ > 400 nm	H_2O: EtOH = 9:1	2
CoPc-BTM-COF	2096 μmol g^{-1} h^{-1}	λ > 400 nm	H_2O: EtOH = 9:1	3
CoPc-DAB-COF	1851μmol g^{-1} h^{-1}	λ > 400 nm	H_2O: EtOH = 9:1	3
EBA-COF	1820μmol g^{-1} h^{-1}	λ = 420 nm	H_2O: EtOH = 9:1	4
CTF-NS-5BT	1630 μmol g^{-1} h^{-1}	λ > 420 nm	H_2O: BA = 9:1	5
COF-TfpBpy	1042 μmol g^{-1}	λ > 420 nm	H_2O	6
TPB-DMTP-COF	606 μmol g^{-1} h^{-1} (O_2-presaturated water)	λ > 420 nm	H_2O	7
	1565 μmol g^{-1} h^{-1} (continuous O_2 bubble)			
CTF-BDDBN	97 μmol g^{-1} h^{-1}	λ > 420 nm	H_2O	8
g-C_3N_4/PDI-BN0.2-$rGO_{0.05}$	30.8 μmol g^{-1} h^{-1}	λ > 420 nm	H_2O	9
Py-Da-COF	1242μmol g^{-1} h^{-1}	λ > 420 nm	H_2O: BA = 9:1	10
TTF-BT-COF	2760 μmol g^{-1} h^{-1}	λ > 420 nm	H_2O	11

Bpy-TAPT	4038 μmol g^{-1} h^{-1}	λ > 420 nm	H_2O	12
FS-COFs	3904 μmol g^{-1} h^{-1}	λ > 420 nm	H_2O	13
TpDz	7327 μmol g^{-1} h^{-1}	λ > 420 nm	H_2O	14
TpMd	6034 μmol g^{-1} h^{-1}	λ > 420 nm	H_2O	14
TpPz	1418 μmol g^{-1} h^{-1}	λ > 420 nm	H_2O	14
TaptBtt COF	1407 μmol g^{-1} h^{-1}	λ > 420 nm	H_2O	15
TAPT-TFPACOFs@Pd ICs	2143 μmol g^{-1} h^{-1}	λ > 420 nm	H_2O	16
TD-COF	4620 μmol g^{-1} h^{-1}	λ > 420 nm	H_2O	17
TAPT-BT-COF	1360 ± 30 μmol g^{-1} h^{-1}	λ > 420 nm	H_2O	This work
TAPB-BT-COF	730 ± 30 μmol g^{-1} h^{-1}	λ > 420 nm	H_2O	This work

Tab. S3 Comparison of reaction rates under different solvent, gas and light conditions.

Entry	**catalyst**	**Solvent system**$_5$	**Gas**	**Irradiation conditions**	**H_2O_2 production rate(umol/g/h)**
1	Blank	Water	O_2	Light	0
2	TAPT-BT-COF	Water	Ar	Light	0
3	TAPT-BT-COF	Water	O_2	Dark	0
4	TAPT-BT-COF	Water	BQ: radical scavenger	Light	0
5	TAPT-BT-COF	Water	$AgNO_3$: electron scavenger	Light	26
6	TAPT-BT-COF	Water	O_2	Light	1363
7	TAPT-BT-COF	Water/EtOH=9:1	O_2	Light	1740
8	TAPT-BT-COF	Water	TBA: hydroxyl radical scavenger	Light	1357

References

1. Krishnaraj, C.; Sekhar Jena, H.; Bourda, L.; Laemont, A.; Pachfule, P.; Roeser, J.; Chandran, C. V.; Borgmans, S.; Rogge, S. M. J.; Leus, K.; Stevens, C. V.; Martens, J. A.; Van Speybroeck, V.; Breynaert, E.; Thomas, A.; Van Der Voort, P., Strongly Reducing (Diarylamino)benzene-Based Covalent Organic Framework for Metal-Free Visible Light Photocatalytic H_2O_2 Generation. *J Am Chem*

Soc **2020,** *142* (47), 20107-20116.
2. Wang, H.; Yang, C.; Chen, F.; Zheng, G.; Han, Q., A Crystalline Partially Fluorinated Triazine Covalent Organic Framework for Efficient Photosynthesis of Hydrogen Peroxide. *Angew Chem Int Ed Engl* **2022,** *61* (19), e202202328.
3. Zhi, Q.; Liu, W.; Jiang, R.; Zhan, X.; Jin, Y.; Chen, X.; Yang, X.; Wang, K.; Cao, W.; Qi, D.; Jiang, J., Piperazine-Linked Metalphthalocyanine Frameworks for Highly Efficient Visible-Light-Driven H_2O_2 Photosynthesis. *J Am Chem Soc* **2022,** *144* (46), 21328-21336.
4. Zhai, L.; Xie, Z.; Cui, C.-X.; Yang, X.; Xu, Q.; Ke, X.; Liu, M.; Qu, L.-B.; Chen, X.; Mi, L., Constructing Synergistic Triazine and Acetylene Cores in Fully Conjugated Covalent Organic Frameworks for Cascade Photocatalytic H_2O_2 Production. *Chem. Mater.* **2022,** *34* (11), 5232-5240.
5. Yu, X.; Viengkeo, B.; He, Q.; Zhao, X.; Huang, Q.; Li, P.; Huang, W.; Li, Y., Electronic Tuning of Covalent Triazine Framework Nanoshells for Highly Efficient Photocatalytic H2O2 Production. *Advanced Sustainable Systems* **2021,** *5* (10).
6. Kou, M.; Wang, Y.; Xu, Y.; Ye, L.; Huang, Y.; Jia, B.; Li, H.; Ren, J.; Deng, Y.; Chen, J.; Zhou, Y.; Lei, K.; Wang, L.; Liu, W.; Huang, H.; Ma, T., Molecularly Engineered Covalent Organic Frameworks for Hydrogen Peroxide Photosynthesis. *Angew Chem Int Ed Engl* **2022,** *61* (19), e202200413.
7. Li, L.; Xu, L.; Hu, Z.; Yu, J. C., Enhanced Mass Transfer of Oxygen through a Gas–Liquid–Solid Interface for Photocatalytic Hydrogen Peroxide Production. *Adv. Funct. Mater.* **2021,** *31* (52).
8. Chen, L.; Wang, L.; Wan, Y.; Zhang, Y.; Qi, Z.; Wu, X.; Xu, H., Acetylene and Diacetylene Functionalized Covalent Triazine Frameworks as Metal-Free Photocatalysts for Hydrogen Peroxide Production: A New Two-Electron Water Oxidation Pathway. *Adv Mater* **2020,** *32* (2), e1904433.
9. Kofuji, Y.; Isobe, Y.; Shiraishi, Y.; Sakamoto, H.; Ichikawa, S.; Tanaka, S.; Hirai, T., Hydrogen Peroxide Production on a Carbon Nitride–Boron Nitride-Reduced Graphene Oxide Hybrid Photocatalyst under Visible Light. *ChemCatChem* **2018,** *10* (9), 2070-2077.
10. Sun, J.; Jena, H. S.; Krishnaraj, C.; Singh Rawat, K.; Abednatanzi, S.; Chakraborty, J.; L aemont, A.; Liu, W.; Chen, H.; Liu, Y.-Y.; Leus, K.; Vrielinck, H.; Van Speybroeck, V.; van der Voort, P., Pyrene-Based Covalent Organic Frameworks for Photocatalytic Hydrogen Peroxide Production. *Angewandte Chemie International Edition n/a* (n/a), e202216719.
11. Chang, J.-N.; Li, Q.; Shi, J.-W., Zhang, M.; Zhang, L., Li, S.; Chen, Y., Li, S.-L.; Lan, Y.-Qc Oxidation-Reduction Molecular Junction Covalent Organic Frameworks for Full Reaction Photosynthesis of H_2O_2. *Angew. Chem.* **2023**, *135*, e202218868.
12. Liu, Y.; Han, W.-K.; Chi, W.; Mao, Y.; Jiang, Y.; Yan, X.; Gu, Z.-G.;Substoichiometric covalent organic frameworks with uncondensed aldehyde for highly efficient hydrogen peroxide photosynthesis in pure water, Applied Catalysis B: Environmental, 2023,122691.
13. Luo, Y.; Zhang, B.; Liu, C.; Xia, D.; Ou, X.; Cai, Y.; Zhou, Y.; Jiang, J.; Han, B., Sulfone-Modified Covalent Organic Frameworks Enabling Efficient Photocatalytic

Hydrogen Peroxide Generation via One-Step TwoElectron O2 Reduction *Angew. Chem. Int. Ed.* 2023, 62, e202305355.
14. Liao, Q.; Sun, Q.; Xu, H., Wang, Y.; Xu, Y.; Li, Z.; Hu, J.; Wang, D.; Li, H.; Xi, K., Regulating Relative Nitrogen Locations of Diazine Functionalized Covalent Organic Frameworks for Overall H_2O_2 Photosynthesis. *Angew. Chem. Int. Ed.* 2023, e202310556.
15. Qin, C.; Wu, X.; Tang, L. *et al.* Dual donor-acceptor covalent organic frameworks for hydrogen peroxide photosynthesis. *Nat Commun* **14**, 5238 (2023).
16. Liu Y.; Li L.; Tan H.; Ye N.; Gu Y.; Zhao S.; Zhang S.; Luo M.; Guo S. Fluorination of Covalent Organic Framework Reinforcing the Confinement of Pd Nanoclusters Enhances Hydrogen Peroxide Photosynthesis. Journal of the American Chemical Society **2023** 145 (36), 19877-19884.
17. Yue, J.-Y.; Song, L.-P.; Fan, Y.-F.; Pan, Z.-X.; Yang, P.; Ma, Y.; Xu, Q.; Tang, B., Thiophene-Containing Covalent Organic Frameworks for Overall Photocatalytic H2O2 Synthesis in Water and Seawater,. *Angew. Chem. Int. Ed. 2023, 62, e202309624.*